PAPER • OPEN ACCESS

Nonlinear electric response of chiral topological superconductors

To cite this article: Minchul Lee and Rosa Lpez 2021 *New J. Phys.* **23** 043009

New Journal of Physics
The open access journal at the forefront of physics

Deutsche Physikalische Gesellschaft DPG
IOP Institute of Physics

Published in partnership with: Deutsche Physikalische Gesellschaft and the Institute of Physics

OPEN ACCESS

RECEIVED
14 September 2020

REVISED
25 December 2020

ACCEPTED FOR PUBLICATION
5 January 2021

PUBLISHED
2 April 2021

PAPER

Nonlinear electric response of chiral topological superconductors

Minchul Lee[1] **and Rosa López**[2,*]

[1] Department of Applied Physics and Institute of Natural Science, College of Applied Science, Kyung Hee University, Yongin 17104, Republic of Korea
[2] Institut de Física Interdisciplinària i de Sistemes Complexos IFISC (CSIC-UIB), E-07122 Palma de Mallorca, Spain
[*] Author to whom any correspondence should be addressed.

E-mail: rosa.lopez-gonzalo@uib.es

Keywords: topological systems, quantum dots, time-dependent transport, dissipation

Abstract

We investigate, in the non-equilibrium Keldysh frame, a topological resistor–capacitor (RC) circuit consisting of a quantum dot coupled to a Majorana edge mode formed around a chiral topological superconductor. We implement both the adiabatic approximation and the numerical exact calculations to find out the unique non-equilibrium features of the electric response of the dissipative Majorana channel. First, the dependence of the dissipation on the frequency Ω of the ac driving on the dot is found to be greatly different whether the time-dependent dot level crosses the Fermi level or not during the driving. In the latter case, the relaxation resistance R_q, the measure of the dissipation, obeys $R_q \propto \Omega^2$ for small frequencies, and in the former case, $R_q \propto \Omega^{-1/3}$ diverges as $\Omega \to 0$. In the former case, a universal scaling law for the dissipative part of the ac power is observed and attributed to the δ-peak in the dot density of states due to a uncoupled dot Majorana mode at the dot resonance condition. We compare the ac power, current, and the relaxation resistance between Majorana and trivial Dirac channels and clarify the Majorana nature in the dissipation.

1. Introduction

The most characteristic property of topological insulators [1] is that gapless states are formed around their boundaries or at defects while a finite energy gap is fully formed inside their bulk. The surface states, being topologically protected, open nontrivial conducting channels with interesting properties: for example, chiral or helical transport, spin-momentum locking, quantized conductance through them, the relativistic dispersion of massless-Dirac-cone shape, and so on. More interestingly, the surface states for topological superconductors [2] are known to exhibit the properties genuine to Majorana-fermion-like excitations: the creation and annihilation of those excitations are the same [3–7]. The realization and manipulation of long-anticipated Majorana fermions in solid-state systems have attracted a plethora of theoretical and experimental studies. Most of the studies have focused on the one-dimensional (1D) topological superconductor [8] because of the possibility that the Majorana bound states formed at the ends of the wires can be used for the topological quantum computation [9, 10]. A series of experimental studies have been performed to detect the evasive charge-neutral and spinless Majorana states by measuring the zero-bias peak in the density of state [11–18] and observing the ac fractional Josephson effect [19, 20], developing more positive outlook on the realization of the Majorana states.

On the other hand, the two-dimensional topological superconductor [2, 21] can be more interesting because it hosts continuum bands of Majorana states around its boundary, in contrast to the localized and discrete ones in the 1D case. The typical gapped superconductor can support dissipationless supercurrent as long as quasiparticle excitations above the gap are not involved. The Majonara boundary modes, however, can be regarded as gapless quasiparticle excitations and should be dissipative even in the presence of the finite bulk gap. Moreover, the Majorana states consist of particle and hole excitations in equal amplitude,

which are topologically protected. This topological nature can give rise to nontrivial behaviors in the transport through the Majorana edge modes [22]. For example, the chiral Majorana edge modes can lead to half-integer quantized conductance through it due to their half-fermionic nature. A recent experiment [23] on a quantum anomalous Hall (QAH) insulator-superconductor structure claimed that the chiral Majorana mode is observed based on its measurement of the half-integer conductance plateaus over some parameter ranges. However, it was found theoretically [24, 25] and experimentally [26] that such plateaus could be observed in similar systems even without superconductivity if some conditions are met. It is evident that more concrete corroboration for the chiral Majorana modes should go beyond the dc measurement.

One of simple but powerful transport setup for studying the electronic dissipation is the quantum capacitor in which one plate of the capacitor consists of a quantum dot and the other is formed by a macroscopic top gate on it. The quantum dot is tunnel-coupled to the metallic reservoir in interest. Such setup was envisaged by Büttiker in references [27, 28] in which the capacitor is described by an equivalent quantum resistor–capacitor (RC) circuit with quantum parameters, i.e. a quantum capacitance C_q and a quantum resistance R_q. The RC device is driven by a time-dependent bias voltage that charges and discharges the capacitor by the elementary charge e. Interestingly, in the quantum limit and in the low-frequency limit the quantum relaxation resistance R_q becomes universal being, half the resistance quantum $R_Q \equiv h/e^2$ per channel, regardless of the transmission between the quantum dot and the reservoir [27–29]. The quantization of the resistance for small ac frequencies persists even in the presence of strong electron–electron interaction (for example, in the Kondo regime), as long as the low-energy physics can be dictated by the Fermi-liquid theory which fulfills the Korringa–Shiba relation [30–34]. The relaxation resistance, therefore, surely reflects the characteristic of spectral structure of the attached metallic reservoir. For example, the low-frequency relaxation resistance should vanish for a superconducting reservoir. The relaxation resistance is attributed to the energy relaxation of particle–hole pair in the reservoir excited by the ac driving [31, 35]. The finite gap in the superconductor forbids the excitation of the electron–hole pair inside the gap, so no relaxation happens. Then, what about the Majorana reservoir? As noted before, the Majorana modes feature both superconductivity (equal amplitudes of particle and hole excitations) and dissipation. Therefore, the relaxation resistance for the Majorana reservoir should be highly nontrivial. It might be worth noting that the similar studies based on the quantum RC circuit have been applied to the quantum-dot systems having the Majorana bound states formed at the ends of 1D topological superconductors [36, 37]. Even though these studies have revealed the genuine effect of the Majorana physics on the transport, the Majorana states in these setups, being discrete bound states, are not main culprit for the dissipation. However, in our RC circuit, the dissipation happens via the dispersive Majorana edge modes, which distinguishes our work from the previous works.

The dissipation in the quantum RC circuit with chiral Majorana reservoir has been studied in the linear response regime [35]. It finds that the relaxation resistance is suppressed for very low frequencies and completely vanishes at zero-frequency limit. It is attributed to the exact cancellation between particle–hole pair generation processes via charge-conserving and pairing tunneling between the dot and the reservoir, reflecting the half-fermionic nature. On the other hand, the exactly same nature of Majorana fermion leads to the enhancement of the relaxation resistance for finite frequencies when the dot level is near the Fermi level, that is, near the resonance condition. On resonance, the density of states in the dot at the Fermi energy increases divergingly, leading to proliferation of the particle–hole pairs. While the linear-response study have investigated well the exotic dissipation via the Majorana edge modes, there remain some limitations. First, the diverging density of states on resonance makes the linear-response theory unreliable, giving rise to quantitatively wrong results as will be shown below. Second, the dissipation in itself involves the non-equilibrium situation which is beyond the linear-response study.

In our study, we apply the non-equilibrium Keldysh formalism to a topological RC circuit consisting of a quantum dot coupled to a chiral Majorana edge mode formed around a chiral topological superconductor. We implement both the adiabatic approximation and the numerical exact calculations to explore the dissipation mechanism via the Majorana channel. We found that the dependence of the dissipation on the frequency Ω of the ac driving is greatly different whether the dot becomes resonant or not during the driving. In the latter case, the relaxation resistance R_q, the measure of the dissipation, obeys $R_q \propto \Omega^2$ for small frequencies, and in the former case, $R_q \propto \Omega^{-1/3}$ diverges as $\Omega \to 0$. Interestingly, for a large ac driving under which the dot level can be shifted to the Fermi level, the dissipative part of the ac power follows a universal scaling law, which can be attributed to the δ-peak in the dot density of states due to a uncoupled dot Majorana mode at the dot resonance. In order to clarify the Majorana nature in the dissipation, we compare the ac power, current, and the relaxation resistance between Majorana and trivial Dirac channels in details.

Our paper is organized as follows: in section 2, our model is introduced and the Keldysh technique is applied to find the exact formulas of the relaxation resistance in terms of the non-equilibrium Green's

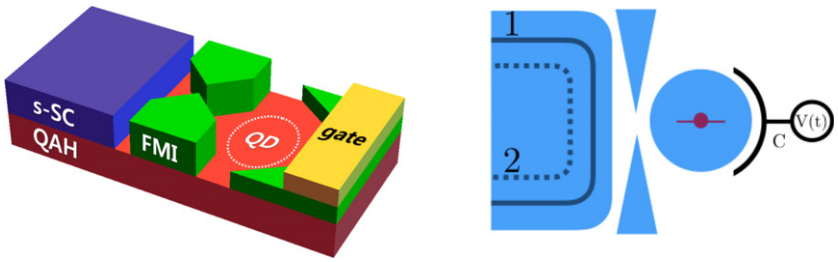

Figure 1. (LEFT) Realization of a quantum RC circuit with chiral topological superconductor coupled to a quantum dot. (RIGHT) Schematic diagram describing the coupling between a spinless dot level and two spatially separated Majorana edge modes ($j = 1, 2$).

functions. For a limiting case study, especially for low-frequency response, we derive the analytical expression in the adiabatic approximation. Also, the recipe for numerical exact solution is described in details. Sections 3 and 4 are the main parts of our paper and give thorough analysis of the current, power, and relaxation resistance for normal metallic reservoir and topological superconducting reservoir. We summarize our work in section 5.

2. Model and methods

The physical implementation of our topological RC circuit is depicted in figure 1. Following the theoretical proposal [21], the chiral topological superconductor can be implemented by depositing a slab of s-wave superconductor on top of a film of QAH insulator. The QAH states can be induced by doping magnetic impurities such as Mn and Cr into films of topological insulators such as HgTe or Bi_2Te_3 [38–40]. As a result, there appear spin-polarized chiral modes along the edges that form a Dirac fermion, which mathematically can be decomposed into two Majorana edge modes ($j = 1, 2$). The transition from two Majorana modes into a half Dirac fermion is brought by placing a s-wave superconductor on top of the topological insulator [21]. The proximity-induced pairing potential places one of the Majorana edge modes (say $j = 2$) towards bulk, and the two edge modes become spatially separated from each other. Finally, this system undergoes a topological phase transition when one of the two Majorana modes lies in the bulk, being gapped now. By placing ferromagnetic insulators on top of the QAH film, one can turn the underneath region into the trivially insulating state, and the boundary of the topological superconductor is located between the superconductor and ferromagnet slabs. Also, a quantum dot can be also formed by confining the QAH region by the ferromagnet-driven insulating region, as shown in figure 1. A tunnel junction between the dot and the Majorana edge mode can be opened by controlling the width of the ferromagnet bar between the dot and the topological superconductor.

Now we present the model Hamiltonian to describe the topological quantum capacitor formed by a quantum dot that is tunnel-coupled to two Majorana edge modes formed around a topological superconductor. The Hamiltonian is composed of the three contributions, namely from the reservoir, the quantum dot and the coupling between them: $\mathcal{H} = \mathcal{H}_{\rm res} + \mathcal{H}_{\rm dot} + \mathcal{H}_{\rm tun}$. Since we focus on the low-energy physics and disregard the bulk dynamics, only the edge modes are responsible for the dissipative reservoir which is described by

$$\mathcal{H}_{\rm res} = \sum_{j=1,2} \sum_{k>0} \epsilon_k \gamma_{-k,j} \gamma_{k,j} = \sum_k \epsilon_k c_k^\dagger c_k, \tag{1}$$

where $\gamma_{k,j} = \gamma_{-k,j}^\dagger$ are chiral Majorana fermion operators with the linear dispersion $\epsilon_k = \hbar v k$, where k is the momentum and v is the propagation velocity of the Majorana edge modes. Here we assume that $k = 0$ is the Γ point in 1D Brillouin zone [21] for the Majorana edge mode, while this is not required for the QAH edge mode. The linear combination of the two Majorana fermions can construct the chiral and spinless Dirac fermion operators $c_k \equiv (\gamma_{k,1} + i\gamma_{k,2})/\sqrt{2}$. In the single Majorana case we keep only $j = 1$ mode, while $j = 2$ mode disappears into the bulk. Since the QAH state is already spin-polarized, the quantum dot can be described in terms of a single spinless level $\epsilon_{\rm d}$:

$$H_{\rm dot} = [\epsilon_{\rm d} + eV(t)]\, d^\dagger d \equiv \epsilon_{\rm d}(t) d^\dagger d. \tag{2}$$

Here the time-dependent induced ac voltage $V(t) = V_{\rm ac} \cos \Omega t$ incorporates the external gate voltage and the induced internal potential due to the geometrical capacitance between the dot and the gate.

The coupling of the dot level to the chiral Majorana edge modes ($j = 1, 2$) with separate spatial localizations takes a tunneling model [22]

$$H_{\rm tun} = \sum_k \left[t_1 d^\dagger \gamma_{k,1} + i t_2 d^\dagger \gamma_{k,2} + ({\rm h.c.}) \right], \tag{3}$$

in terms of the tunneling amplitudes t_j between the Majorana mode j and the dot level. For simplicity, we neglects the momentum dependence of the tunneling amplitudes. In terms of the Dirac fermion operator, the tunneling Hamiltonian is expressed as

$$H_{\rm tun} = \sum_k \left[t_+ d^\dagger c_k + t_- d^\dagger c_k^\dagger + ({\rm h.c.}) \right] \tag{4}$$

with $t_\pm \equiv (t_1 \pm t_2)/\sqrt{2}$. The first term ($t_+$) represents the normal single-electron tunneling between the dot and the reservoir, while the second one (t_-) describes the creation of a Cooper pair from the dot and the reservoir. One can note that if the two Majorana edge modes share the same spatial distribution so that $t_1 = t_2$ or $t_- = 0$, the system exhibits no superconductivity, restoring the QAH case. Assuming the flat band structure in the reservoir, the coupling is conveniently described by the hybridization parameters $\Gamma_j \equiv \pi \rho_0 |t_j|^2/\hbar$ with the density of states $\rho_0 = 1/2\pi\hbar v$. Due to spatially separated localizations of the two Majorana modes, $\Gamma_1 \geqslant \Gamma_2$; in particular, $\Gamma_1 = \Gamma_2$ only in the QAH phase and $\Gamma_2 = 0$ in the chiral topological superconducting (cTSC) phase.

Note that our model ignores the bulk states of the reservoir. Therefore, $\hbar\Gamma_j$, $eV_{\rm ac}$, and $\hbar\Omega$ should be sufficiently smaller than the bulk (superconducting) gap so that the ac driving in the gate does not invoke the quasi-particle excitation in the bulk.

2.1. Electrical current and power in terms of non-equilibrium Green's functions

Our interest lies on the study of charge current and energy dissipation with respect to the ac driving with arbitrary frequency and amplitude. Knowing the time dependence of the dot occupation

$$n_{\rm d}(t) = \left\langle d^\dagger(t) d(t) \right\rangle \tag{5}$$

one can obtain the charge current from the dot to the reservoir via [41]

$$I(t) = -e \frac{{\rm d}n_{\rm d}(t)}{{\rm d}t}. \tag{6}$$

Note that the dot is tunnel-coupled to the reservoir so that the charge current can flow into the reservoir only. Also, this current should be equal to the displacement current in magnitude between the dot and the gate, so the current can be measured by observing the ac current through the gate. The power supplied by the ac source is given by

$$P(t) = -\left\langle \frac{\partial \mathcal{H}}{\partial t} \right\rangle = -e \frac{{\rm d}V(t)}{{\rm d}t} n_{\rm d}(t) \tag{7}$$

which also measures the dissipation $\dot{Q} = -P(t)$ in the reservoir [42].

In order to calculate the above quantities in the non-equilibrium condition, one needs to introduce the Nambu–Keldysh Green functions. The lesser dot Green function in the Nambu space is defined by

$$-i\mathcal{G}_{\rm d}^<(t,t') = \begin{bmatrix} \langle d^\dagger(t') d(t) \rangle & \langle d(t') d(t) \rangle \\ \langle d^\dagger(t') d^\dagger(t) \rangle & \langle d(t') d^\dagger(t) \rangle \end{bmatrix} \tag{8}$$

and the other Green functions such as $\mathcal{G}_{\rm d}^>$, $\mathcal{G}_{\rm d}^t$, and $\mathcal{G}_{\rm d}^{\bar{t}}$ are defined accordingly. Then, the dot occupation can be obtained via $n_d(t) = -i[\mathcal{G}_d^<(t,t)]_{11}$. By using the equation-of-motion technique, it is quite straightforward to derive the Dyson's equation

$$\begin{aligned} \widehat{\mathcal{G}}_{\rm d}(t,t') = \widehat{g}_{\rm d}(t,t') &+ \int {\rm d}t'' \widehat{\mathcal{G}}_{\rm d}(t,t'') \mathcal{V}(t'') \tau_3 \widehat{g}_{\rm d}(t'',t') \\ &+ \int {\rm d}t'' \int {\rm d}t''' \widehat{\mathcal{G}}_{\rm d}(t,t'') \tau_3 \widehat{\Sigma}(t'',t''') \tau_3 \widehat{g}_{\rm d}(t''',t') \end{aligned} \tag{9}$$

for the dot Green function

$$\widehat{\mathcal{G}}_{\rm d}(t,t') = \begin{bmatrix} \mathcal{G}_{\rm d}^t(t,t') & \mathcal{G}_{\rm d}^<(t,t') \\ \mathcal{G}_{\rm d}^>(t,t') & \mathcal{G}_{\rm d}^{\bar{t}}(t,t'), \end{bmatrix} \tag{10}$$

where τ_i $(i = 1, 2, 3)$ are the Pauli matrices in the Keldysh space. Here $\widehat{g}_{\rm d}(t, t') = \widehat{g}_{\rm d}(t - t')$ is the unperturbed dot Green function in the *absence* of the ac driving. The ac driving enters into the Dyson's equation via the term

$$\mathcal{V}(t) \equiv \frac{e}{\hbar} V(t)\sigma_3 \equiv v(t)\sigma_3 \tag{11}$$

where σ_i $(i = 0, 1, 2, 3)$ are the Pauli matrices in the Nambu space. The derivation introduces the self energy

$$\widehat{\Sigma}(t, t') = \widehat{\Sigma}(t - t') = \sum_k \frac{\mathcal{T}^\dagger}{\hbar} \widehat{g}_k(t - t') \frac{\mathcal{T}}{\hbar} \tag{12}$$

in terms of the unperturbed reservoir Green function $\widehat{g}_k(t - t')$ (defined with respect to $\mathcal{H}_{\rm res}$) and the dot-reservoir coupling matrix

$$\mathcal{T} \equiv \begin{bmatrix} t_+^* & -t_- \\ t_-^* & -t_+ \end{bmatrix}. \tag{13}$$

Direct calculation, assuming the flat-band structure in the reservoir, gives rise to the Fourier components of the self energies,

$$\Sigma^{\rm R/A}(\omega) = \mp i\Gamma \quad \text{and} \quad \Sigma^{<}(\omega) = 2if(\hbar\omega)\Gamma, \tag{14}$$

where $f(\epsilon = \hbar\omega)$ is the Fermi–Dirac distribution function and $\Gamma(\omega) \equiv \frac{\pi}{\hbar}\sum_k \mathcal{T}^\dagger \delta(\hbar\omega - \epsilon_k\sigma_3)\mathcal{T}$ is the matrix of escaping rate given by

$$\Gamma = \begin{bmatrix} \Gamma_n & \Gamma_a \\ \Gamma_a & \Gamma_n \end{bmatrix} \quad \text{with} \quad \Gamma_{n/a} \equiv \frac{\Gamma_2 \pm \Gamma_1}{2}. \tag{15}$$

For calculating explicitly the dot Green function needed for the charge current it is useful to define the mixed spectral representation since the ac driving is periodic with a period $\tau = 2\pi/\Omega$ and the Green functions should reflect the same periodicity:

$$\mathcal{G}(n, \omega) = \frac{1}{\tau}\int_0^\tau {\rm d}t\, {\rm e}^{{\rm i}n\Omega t}\mathcal{G}(t, \omega), \qquad \mathcal{G}(t, \omega) = \int {\rm d}t'\, {\rm e}^{{\rm i}\omega(t-t')}\mathcal{G}(t, t'), \tag{16}$$

and inversely

$$\mathcal{G}(t, t') = \int \frac{{\rm d}\omega}{2\pi}\, {\rm e}^{-{\rm i}\omega(t-t')}\mathcal{G}(t, \omega), \qquad \mathcal{G}(t, \omega) = \sum_n \mathcal{G}(n, \omega){\rm e}^{-{\rm i}n\Omega t}. \tag{17}$$

Also, the Fourier components of the ac driving are similarly defined as

$$v_n = \frac{1}{\tau}\int_0^\tau {\rm d}t\, {\rm e}^{{\rm i}\Omega t} v(t). \tag{18}$$

Rewriting the Dyson's equation, equation (9), in the mixed spectral representation, one finds recurrence relations for the retarded/advanced dot Green functions:

$$\mathcal{G}_{\rm d}^{\rm R/A}(n, \omega) = \left(\delta_{n,0}\sigma_0 + \sum_{n'} \mathcal{G}_{\rm d}^{\rm R/A}(n - n', \omega + n'\Omega)\mathcal{V}_{n'}\right) \mathcal{G}_{\rm d,0}^{\rm R/A}(\omega) \tag{19}$$

with $\mathcal{V}_n \equiv \sigma_3 v_n$ and the retarded/advanced dot Green functions in the absence of ac driving

$$\mathcal{G}_{\rm d,0}^{\rm R/A}(\omega) = \left([g_{\rm d}^{\rm R/A}(\omega)]^{-1} - \Sigma^{\rm R/A}(\omega)\right)^{-1}. \tag{20}$$

Similarly, the lesser dot Green function in the mixed spectral representation is found to satisfy

$$\mathcal{G}_{\rm d}^{<}(n, \omega) = \left(\sum_{n'} \mathcal{G}_{\rm d}^{<}(n - n', \omega + n'\Omega)\mathcal{V}_{n'} + \mathcal{G}_{\rm d}^{\rm R}(n, \omega)\Sigma^{<}(\omega)\right) \mathcal{G}_{\rm d,0}^{\rm A}(\omega). \tag{21}$$

By solving equations (19) and (21), one can compute the dot occupation and subsequently the charge current and energy dissipation. In the following sections, we present analytical and numerical methods to solve equations (19) and (21).

2.2. Adiabatic approximation

Unfortunately, no exact analytical solutions to equations (19) and (21) are available, so some limiting approximation should be assumed. Here we introduce the adiabatic approximation which takes the ac

quantum energy $\hbar\Omega$ as the smallest one compared to other energy scales in the system such as $\hbar\Gamma_i$ and $eV_{\rm ac}$ and so on. Here we expand the Fourier components of dot Green functions with respect to Ω, accordingly

$$\mathcal{G}_{\rm d}(n,\omega) = \mathcal{G}^{\rm f}_{\rm d}(n,\omega) + \Omega\mathcal{G}^{(1)}_{\rm d}(n,\omega) + \mathcal{O}(\Omega^2) \tag{22a}$$

$$\mathcal{G}_{\rm d}(n,\omega+n'\Omega) = \mathcal{G}^{\rm f}_{\rm d}(n,\omega) + \Omega\left(n'\partial_\omega\mathcal{G}^{\rm f}_{\rm d}(n,\omega) + \mathcal{G}^{(1)}_{\rm d}(n,\omega)\right) + \mathcal{O}(\Omega^2), \tag{22b}$$

where the zeroth-order term, $\mathcal{G}^{\rm f}_{\rm d}$ is named as the *frozen* Green's function. By substituting the Green functions in equations (19) and (21) by equation (22), one can set up the self-consistent equations for $\mathcal{G}^{\rm f}_{\rm d}$ and $\mathcal{G}^{(1)}_{\rm d}$. The frozen Green functions are obtained as

$$\mathcal{G}^{\rm R/A,f}_{\rm d}(t,\omega) = \left[\omega - (\epsilon_{\rm d}/\hbar + v(t))\sigma_3 - \Sigma^{\rm R/A}(\omega)\right]^{-1}, \tag{23a}$$

$$\mathcal{G}^{<,{\rm f}}_{\rm d}(t,\omega) = \mathcal{G}^{\rm R,f}_{\rm d}(t,\omega)\Sigma^{<}(\omega)\mathcal{G}^{\rm A,f}_{\rm d}(t,\omega). \tag{23b}$$

These are basically the *equilibrium* Green functions except the fact that the dot level is now time-dependent, $\epsilon_{\rm d}(t)$. This is truly adiabatic solution in that, since the time variation is slow enough, at every moment the system is in equilibrium with respect to the dot level at the moment. The self-consistent equations for the first-order terms are

$$\mathcal{G}^{R,(1)}_{\rm d}(n,\omega) = \sum_{n'}\left[n'\partial_\omega\mathcal{G}^{\rm R,f}_{\rm d}(n-n',\omega) + \mathcal{G}^{R,(1)}_{\rm d}(n-n',\omega)\right]\mathcal{V}_{n'}\mathcal{G}^{\rm R}_{\rm d,0}(\omega), \tag{24a}$$

$$\mathcal{G}^{<,(1)}_{\rm d}(n,\omega) = \left[\sum_{n'}\left(n'\partial_\omega\mathcal{G}^{<,{\rm f}}_{\rm d}(n-n',\omega) + \mathcal{G}^{<,(1)}_{\rm d}(n-n',\omega)\right)\mathcal{V}_{n'} + \mathcal{G}^{R,(1)}_{\rm d}(n,\omega)\Sigma^{<}(\omega)\right]\mathcal{G}^{\rm A}_{\rm d,0}(\omega). \tag{24b}$$

These equations can be solved by applying the inverse Fourier transformation, giving rise to the resulting Green functions

$$\mathcal{G}^{\rm R}_{\rm d}(t,\omega) \approx \mathcal{G}^{\rm R,f}_{\rm d}(t,\omega) + i\partial_\omega\mathcal{G}^{\rm R,f}_{\rm d}(t,\omega)\frac{{\rm d}\mathcal{V}(t)}{{\rm d}t}\mathcal{G}^{\rm R,f}_{\rm d}(t,\omega), \tag{25a}$$

$$\mathcal{G}^{<}_{\rm d}(t,\omega) \approx \mathcal{G}^{<,{\rm f}}_{\rm d}(t,\omega) + i\left[\partial_\omega\mathcal{G}^{<,{\rm f}}_{\rm d}(t,\omega)\frac{{\rm d}\mathcal{V}(t)}{{\rm d}t}\mathcal{G}^{\rm A,f}_{\rm d}(t,\omega) + \partial_\omega\mathcal{G}^{\rm R,f}_{\rm d}(t,\omega)\frac{{\rm d}\mathcal{V}(t)}{{\rm d}t}\mathcal{G}^{<,{\rm f}}_{\rm d}(t,\omega)\right]. \tag{25b}$$

For later use, we define the frozen dot density of states, $\rho^{\rm f}_{\rm d}(t,\omega)$ as

$$\rho^{\rm f}_{\rm d}(t,\omega) = -\frac{1}{\pi\hbar}\,{\rm Im}\,\mathcal{G}^{\rm R,f}_{\rm d}(t,\omega). \tag{26}$$

Since the frozen Green functions satisfy the same properties as the equilibrium ones do, the following relation holds

$$\mathcal{G}^{<,{\rm f}}_{\rm d}(t,\omega) = i(2\pi\hbar)f(\hbar\omega)\rho^{\rm f}_{\rm d}(t,\omega). \tag{27}$$

Using the dot Green functions in the adiabatic limit and the frozen density of states, the occupation $n_{\rm d}(t) \approx n^{(0)}_{\rm d}(t) + n^{(1)}_{\rm d}(t)$ are found to be

$$n^{(0)}_{\rm d}(t) = \int {\rm d}\epsilon f(\epsilon)[\rho^{\rm f}_{\rm d}(t,\omega)]_{11} \tag{28a}$$

$$n^{(1)}_{\rm d}(t) = e\pi\hbar\int {\rm d}\epsilon\left(-\frac{\partial {\rm f}}{\partial\epsilon}\right)\left([\rho^{\rm f}_{\rm d}(t,\omega)]^2_{11} - [\rho^{\rm f}_{\rm d}(t,\omega)]^2_{12}\right)\dot{V}(t) \tag{28b}$$

and accordingly, the charge current $I(t) \approx I^{(1)}(t) + I^{(2)}(t)$ is found to be

$$I^{(1)}(t) = e^2\int {\rm d}\epsilon\left[\left(-\frac{\partial f}{\partial\epsilon}\right)[\rho^{\rm f}_{\rm d}(t,\omega)]_{11} - f(\epsilon){\rm Im}\left[\frac{2}{\pi\hbar^2}[G^{\rm R,f}_{\rm d}(t,\omega)]^2_{12}\right]\right]\dot{V} \tag{29a}$$

$$I^{(2)}(t) = -e^2\pi\hbar\int {\rm d}\epsilon\left(-\frac{\partial f}{\partial\epsilon}\right)\partial_t\left[\left([\rho^{\rm f}_{\rm d}(t,\omega)]^2_{11} - [\rho^{\rm f}_{\rm d}(t,\omega)]^2_{12}\right)\dot{V}\right]. \tag{29b}$$

The total power supplied by the ac source, equation (7) is then easy to compute so that $P(t) = P_{\rm con}(t) + P_{\rm dis}(t)$ with $P_{\rm con}(t) = en^{\rm f}_{\rm d}(t)\dot{V}(t)$, and $P_{\rm dis}(t) = en^{(1)}_{\rm d}(t)\dot{V}(t)$. Besides, when time-average $\overline{P}(\Omega) = \frac{1}{\tau}\int_0^\tau {\rm d}t\,P(t)$ is considered, the conservative power vanishes, $\overline{P}_{\rm con}(\Omega) = 0$. This is the purely ac component associated with the reversible energy produced by a conservative force. On the contrary, the dissipative

power $\overline{P}(\Omega) = \overline{P}_{\rm dis}(\Omega) \geqslant 0$. From the average dissipative power and the time-average charge current the charge relaxation resistance is obtained via

$$R_{\rm q}(\Omega) = \frac{\overline{P}(\Omega)}{\overline{I^2}(\Omega)}. \tag{30}$$

2.3. Numerical exact solution

Since the adiabatic approximation is valid only for sufficiently slow ac fields we provides here the guidelines about how to addresses the previous calculations for the charge current and ac power by numerical integration. Using the Dyson's equation, equation (9), one can express $\mathcal{G}^<_{\rm d}(t,t')$ in terms of $\mathcal{G}^{\rm R}_{\rm d}(t,t')$ as

$$\mathcal{G}^<_{\rm d}(t,t') = \int {\rm d}t'' \int {\rm d}t''' \mathcal{G}^{\rm R}_{\rm d}(t,t'')\Sigma^<(t'',t''')\mathcal{G}^{\rm A}_{\rm d}(t''',t') \tag{31}$$

so that the equal-time lesser dot Green function is found to be

$$\mathcal{G}^<_{\rm d}(t,t) = \int \frac{{\rm d}\omega}{2\pi} \mathcal{G}^{\rm R}_{\rm d}(t,\omega)\Sigma^<(\omega)[\mathcal{G}^{\rm R}_{\rm d}(t,\omega)]^\dagger. \tag{32}$$

Since $n_{\rm d}(t) = -i[\mathcal{G}^<_{\rm d}(t,t)]_{11}$ and $I(t) = -e\dot{n}_{\rm d}(t)$, one can find the formulas for the occupation and the charge current in terms of $\mathcal{G}^{\rm R}_{\rm d}(t,\omega)$:

$$n_{\rm d}(t) = \int \frac{{\rm d}\omega}{2\pi} f(\hbar\omega)\left[\mathcal{G}^{\rm R}_{\rm d}(t,\omega)(2\Gamma)[\mathcal{G}^{\rm R}_{\rm d}(t,\omega)]^\dagger\right]_{11} \tag{33a}$$

$$I(t) = -2e \int \frac{{\rm d}\omega}{2\pi} f(\hbar\omega){\rm Re}\left[\partial_t\mathcal{G}^{\rm R}_{\rm d}(t,\omega)(2\Gamma)[\mathcal{G}^{\rm R}_{\rm d}(t,\omega)]^\dagger\right]_{11} \tag{33b}$$

The closed-form equation for $\mathcal{G}^{\rm R}_{\rm d}(t,\omega)$ and $\partial_t\mathcal{G}^{\rm R}_{\rm d}(t,\omega)$ can be found by applying the inverse Fourier transformation to the recurrence relation for $\mathcal{G}^{\rm R}_{\rm d}(n,\omega)$, equation (19):

$$\mathcal{G}^{\rm R}_{\rm d}(t,\omega)[\mathcal{G}^{\rm R}_{\rm d,0}(\omega)]^{-1} = \sigma_0 + \sum_{n'} \mathcal{G}^{\rm R}_{\rm d}(t,\omega+n'\Omega)\mathcal{V}_{n'}\,{\rm e}^{-{\rm i}n'\Omega t} \tag{34a}$$

$$\partial_t\mathcal{G}^{\rm R/A}_{\rm d}(t,\omega)[\mathcal{G}^{\rm R/A}_{\rm d,0}(\omega)]^{-1} = \sum_{n'} \left(\partial_t\mathcal{G}^{\rm R/A}_{\rm d}(t,\omega+n'\Omega) - in'\Omega\mathcal{G}^{\rm R/A}_{\rm d}(t,\omega+n'\Omega)\right)\mathcal{V}_{n'}\,{\rm e}^{-{\rm i}n'\Omega t}. \tag{34b}$$

These are coupled linear equations for $\mathcal{G}^{\rm R}_{\rm d}(t,\omega+n\Omega)$ and $\partial_t\mathcal{G}^{\rm R}_{\rm d}(t,\omega+n\Omega)$ for all integer n, respectively, at given t and $0 \leqslant \omega < \Omega$. The dimensions of the linear equations, being infinite, can be made finite by noting that in the large $|\omega|$ limit the solutions can be well approximated by

$$\mathcal{G}^{\rm R}_{\rm d}(t,\omega) \approx \mathcal{G}^{\rm R,f}_{\rm d}(t,\omega) \quad \text{and} \quad \partial_t\mathcal{G}^{\rm R}_{\rm d}(t,\omega) \approx \partial_t\mathcal{G}^{\rm R,f}_{\rm d}(t,\omega). \tag{35}$$

We choose two integers N_1 and $N_2(>0)$ properly so that for $\omega < N_1\Omega$ and $N_2\Omega < \omega$, the dot Green functions are replaced by corresponding approximated values, equation (35), and the $2(N_2-N_1+1)\times 2(N_2-N_1+1)$ coupled linear equations are directly solved to obtain $\mathcal{G}^{\rm R}_{\rm d}(t,\omega_m+n\Omega)$ and $\partial_t\mathcal{G}^{\rm R}_{\rm d}(t,\omega_m+n\Omega)$ for $N_1 \leqslant n \leqslant N_2$. This process is repeated for discrete values of $\omega_m = m\delta\omega$ $(m=0,\ldots,M-1)$, where the frequency spacing $\delta\omega \equiv \Omega/M$ is chosen to be sufficiently small, and for properly chosen discrete times t. Then, the occupation and the current, equation (33), at *zero* temperature can be computed numerically by summing over discrete frequencies via

$$n_{\rm d}(t) = \sum_{N_1\Omega\leqslant\omega_n\leqslant 0} \frac{\delta\omega}{\pi}\left[\mathcal{G}^{\rm R}_{\rm d}(t,\omega_n)\Gamma[\mathcal{G}^{\rm R}_{\rm d}(t,\omega_n)]^\dagger\right]_{11} + n_{\rm d,c}(t) \tag{36a}$$

$$I(t) = -2e \sum_{N_1\Omega\leqslant\omega_n\leqslant 0} \frac{\delta\omega}{\pi}\,{\rm Re}\left[\partial_t\mathcal{G}^{\rm R}_{\rm d}(t,\omega_n)\Gamma\mathcal{G}^{R\dagger}_{\rm d}(t,\omega_n)\right]_{11} + I_{\rm c}(t), \tag{36b}$$

where the correction terms $n_{\rm d,c}(t) = \int_{-\infty}^{N_1\Omega} {\rm d}\epsilon\,[\rho^{\rm f}_{\rm d}(t,\omega)]_{11}$ and $I_{\rm c}(t) = -e\dot{n}_{\rm d,c}(t)$ can be analytically calculated by using the frozen dot Green functions, equation (35). The conservative and dissipative parts of the power $P(t)$, equation (7), are identified by their parity nature, odd and even with respect to the time, respectively:

$$P_{\rm con}(t) = \frac{P(t)-P(\tau-t)}{2} \quad \text{and} \quad P_{\rm dis}(t) = \frac{P(t)+P(\tau-t)}{2}, \tag{37}$$

leading to $\overline{P}_{\rm con} = 0$ and $\overline{P}_{\rm dis} \geqslant 0$.

2.4. Gauge transformation

It is instructive to consider a unitary transformation of the Hamiltonian in order to examine the scope in which the non-equilibrium condition is important. We introduce a gauge transformation defined in terms of a unitary operator $\mathcal{U} = \exp[\frac{i}{\hbar}\mathcal{S}(t)]$ where

$$\mathcal{S}(t) = \int^t \mathrm{d}t' eV(t') d^\dagger d. \tag{38}$$

Under the transformation, the Hamiltonian $\mathcal{H}$ is changed into $\mathcal{H}' = \mathcal{U}\mathcal{H}\mathcal{U}^\dagger - \partial_t \mathcal{S}(t)$. While $\mathcal{H}_{\rm res}$ is invariant, two changes happen: (1) the time-dependent part in the dot Hamiltonian is eliminated: $\mathcal{H}'_{\rm dot} = \epsilon_{\rm d} d^\dagger d$ and (2) the reservoir-dot tunneling amplitudes acquire a time-dependent phase:

$$t_\pm \to t_\pm \, \mathrm{e}^{\mathrm{i}\int^t \mathrm{d}t' \, v(t')} = t_\pm \, \mathrm{e}^{\mathrm{i}\frac{eV_{\rm ac}}{\hbar\Omega} \sin \Omega t}. \tag{39}$$

In the gauge-transformed Hamiltonian $\mathcal{H}'$, the ac amplitude $V_{\rm ac}$ appears *only* in the form of the ratio $V_{\rm ac}/\Omega$. That is, it is the ratio $V_{\rm ac}/\Omega$, not $V_{\rm ac}$ that does matter physically. Using this fact, one can argue that in the large Ω limit the response to the ac driving is well captured by the linear-response theory. Note that the linear-response theory, treating the ac driving as a perturbation, takes the $V_{\rm ac} \to 0$ limit. In this limit the ratio $V_{\rm ac}/\Omega$, the only physically relevant parameter, is very small. Interestingly this small ratio can be also achieved by taking $\Omega \to \infty$ limit. It proves our argument mentioned above. In the next sections, the exact calculations confirm this clearly. So, the effect peculiar to the non-equilibrium condition should occur in the small and intermediate Ω regimes. The adiabatic limit, taking $\Omega \to 0$ limit, is surely expected to display the non-equilibrium features of the system.

3. Results: case of the QAH reservoir

In this section we consider the reservoir in the QAH phase, where the dot-reservoir hybridizations are set to be $\Gamma_1 = \Gamma_2 \equiv \Gamma$. We briefly review the adiabatic limit of this case which was already studied in reference [42] and present the numerical analysis for general non-equilibrium case.

3.1. Adiabatic limit

For the QAH reservoir, the frozen dot density of states has a simple form

$$[\rho^{\rm f}_{\rm d}(t,\omega)]_{11} = \frac{1}{\pi\hbar}\frac{\Gamma}{(\omega - \omega_{\rm d}(t))^2 + \Gamma^2} \quad \text{and} \quad [\rho^{\rm f}_{\rm d}(t,\omega)]_{12} = 0 \tag{40}$$

having no anomalous term, with $\omega_{\rm d}(t) \equiv \epsilon_{\rm d}(t)/\hbar$. The dot occupation and the charge current at zero temperature, equations (28) and (29) are then readily found to be

$$n^{(0)}_{\rm d}(t) = \frac{1}{2} - \frac{1}{\pi}\tan^{-1}\frac{\omega_{\rm d}(t)}{\Gamma} \quad \text{and} \quad n^{(1)}_{\rm d}(t) = \frac{e}{\pi\hbar}\dot{V}(t)\left(\frac{\Gamma}{[\omega_{\rm d}(t)]^2 + \Gamma^2}\right)^2 \tag{41a}$$

$$I^{(1)}(t) = \frac{e^2}{\pi\hbar}\dot{V}(t)\frac{\Gamma}{[\omega_{\rm d}(t)]^2 + \Gamma^2}. \tag{41b}$$

Interestingly, the dissipative part of the power, $P_{\rm dis}(t)$ up to the second order of Ω satisfies the *instantaneous Joule law* at any time t [42]:

$$P_{\rm dis}(t) = e n^{(1)}_{\rm d}(t)\dot{V}(t) = R_{\rm q}[I^{(1)}(t)]^2 \tag{42}$$

with the quantized relaxation resistance $R_{\rm q} = e^2/2h = R_{\rm Q}/2$. It should be noted that the instantaneous Joule law is satisfied for arbitrary values of the dot level $\epsilon_{\rm d}$ and the ac amplitude $V_{\rm ac}$. In particular, it is quite interesting that the relaxation resistance obtained in the linear-response regime ($V_{\rm ac} \to 0$) is still valid in deep non-equilibrium regime.

3.2. Numerical calculation

Numerical calculations find out that the instantaneous Joule law does not hold for finite frequencies. Therefore, we examine the time-averaged values, $\overline{I^2}(\Omega)$ and $\overline{P}(\Omega)$, whose dependence on $v_{\rm ac}$ and Ω are displayed in figure 2. For sufficiently small frequencies, the numerical fitting confirms that the results in the adiabatic approximation, equations (41) and (42) are in good agreement with the exact numerical calculations. Specifically, the numerical calculations for small frequencies find

$$\overline{I^2}(\Omega) \approx 2e^2 c_{\rm QAH}(v_{\rm ac}) v^2_{\rm ac}\left(\frac{\Omega}{2\Gamma}\right)^2 \quad \text{and} \quad \overline{P}(\Omega) \approx h c_{\rm QAH}(v_{\rm ac}) v^2_{\rm ac}\left(\frac{\Omega}{2\Gamma}\right)^2 \tag{43}$$

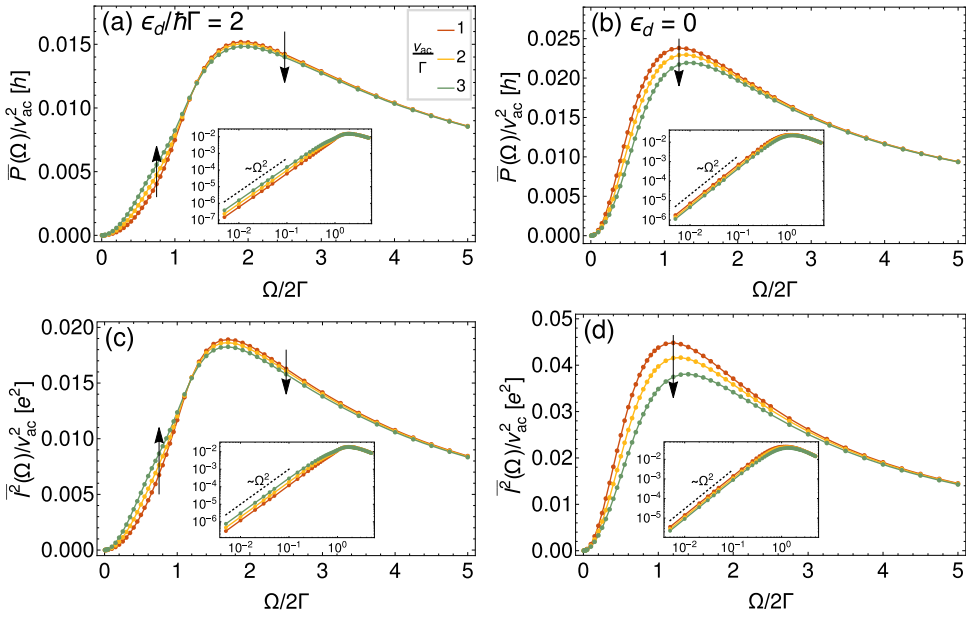

Figure 2. (a) and (b) Time-averaged ac power $\overline{P}/v_{ac}^2$ and (c) and (d) time-averaged squared current $\overline{I^2}/v_{ac}^2$ as functions of Ω for several values of v_{ac} for (a) and (c) $\epsilon_d = 2\hbar\Gamma$ and (b) and (d) $\epsilon_d = 0$ with respect to the QAH reservoir. The arrow indicates the direction along which the chosen values of $v_{ac}/\Gamma = 1, 2, 3$ increases as shown in the legend. The insets show the corresponding logarithmic plots.

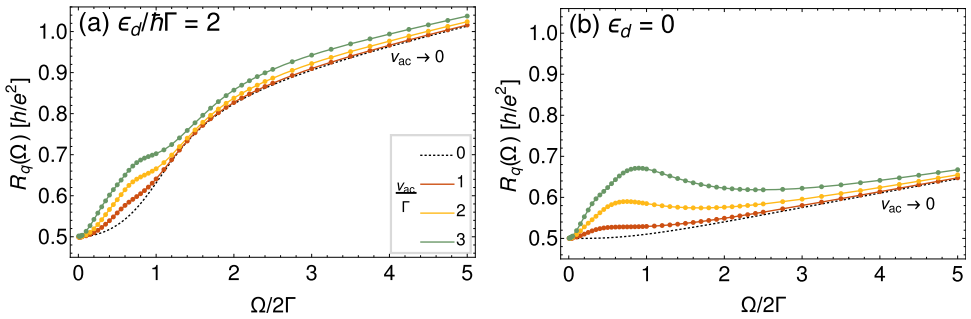

Figure 3. Relaxation resistance R_q as a function of Ω for several values of v_{ac}/Γ as annotated for (a) $\epsilon_d = 2\hbar\Gamma$ and (b) $\epsilon_d = 0$, obtained by using the data in figure 2. The black dotted line represents the linear-response result ($v_{ac} \to 0$).

with the dimensionless constant

$$c_{QAH}(v_{ac}) \equiv \frac{2}{\pi^2}\int_0^\tau \frac{dt}{\tau}\left(\frac{\Gamma^2 \sin \Omega t}{[\omega_d(t)]^2 + \Gamma^2}\right)^2. \tag{44}$$

For $\epsilon_d = 0$, $c_{QAH} = \Gamma/\pi^2\sqrt{\Gamma^2 + v_{ac}^2}$, which explains the decrease of the normalized power $\overline{P}/v_{ac}^2$ with increasing v_{ac} [see figures 2(b) and (d)].

For finite frequencies, both $\overline{P}$ and $\overline{I^2}$ increase monotonically with increasing ac amplitude V_{ac}. On the other hand, they exhibit non-monotonic behavior as functions of Ω, having a maximum at $\Omega \sim 2\Gamma$. It means that the dissipation is maximized when the ac frequency is comparable to the dot-reservoir coupling. Also, the dissipation is the larger as the dot level is closer to the Fermi level; compare figures 2(a) and (b).

The relaxation resistance, equation (30), is readily calculated, as can be seen in figure 3. In the $\Omega \to 0$ limit, $R_q(\Omega) = R_Q/2$ for all values of the amplitude V_{ac}, as predicted by the adiabatic approximation. For finite frequencies, on the other hand, $R_q(\Omega)$ increases with increasing V_{ac}. In the intermediate regime of Ω, a kink structure at $\Omega \sim 2\Gamma$ happens, which is more clearly visible for larger amplitude V_{ac}. For large frequencies, all the R_q curves almost *collapse into a single curve*, following the linear-response behavior (marked by $V_{ac} = 0$) for all values of the amplitude V_{ac}. It is exactly as discussed in section 2.4: when the ac source oscillates very fast, the system cannot keep up with it so that the system is effectively in equilibrium, making the linear response theory accessible.

4. Results: case of the cTSC reservoir

In this section, the reservoir is in the cTSC phase where only the one ($\gamma_{k,1}$) of the Majorana channels remains as the edge mode, leading to $\Gamma_2 = 0$. As will be demonstrated, the ac response of the system is found to be critically different, depending on whether the dot can be on resonance ($\epsilon_{\rm d}(t) = 0$) even temporally during the ac driving or not. Let the interval $\mathcal{I}$ be $[\epsilon_{\rm d} - eV_{\rm ac}, \epsilon_{\rm d} + eV_{\rm ac}]$. Then, two physically different cases can be distinguished as follows: (1) for the case $0 \notin \mathcal{I}$, the time-varying dot level never crosses the Fermi level, more specifically either $\epsilon_{\rm d}(t) < 0$ or $0 < \epsilon_{\rm d}(t)$ for all time t, and (2) for the case $0 \in \mathcal{I}$, the dot can be on resonance since $\epsilon_{\rm d} - eV_{\rm ac} \leqslant 0 \leqslant \epsilon_{\rm d} + eV_{\rm ac}$.

4.1. Adiabatic limit

In the cTSC phase, the frozen dot density of states acquires the finite anomalous term as well:

$$[\rho_{\rm d}^{\rm f}(t,\omega)]_{11} = \frac{\Gamma}{2\pi\hbar}\frac{(\omega+\omega_{\rm d}(t))^2}{(\omega^2-[\omega_{\rm d}(t)]^2)^2+(\omega\Gamma)^2},$$
$$[\rho_{\rm d}^{\rm f}(t,\omega)]_{12} = \frac{\Gamma}{2\pi\hbar}\frac{[\omega_{\rm d}(t)]^2-\omega^2}{(\omega^2-[\omega_{\rm d}(t)]^2)^2+(\omega\Gamma)^2}. \tag{45}$$

At zero temperature, equations (28) and (29) give rise to the dot occupation and the charge current given by

$$n_{\rm d}^{(0)}(t) = \frac{1}{2} + \frac{2\omega_{\rm d}(t)}{\pi\Gamma}\eta(t) \quad \text{and} \quad n_{\rm d}^{(1)}(t) = 0 \tag{46a}$$

$$I^{(1)}(t) = \frac{e^2}{2\pi\hbar}\dot{V}(t)\frac{4\Gamma}{[2\omega_{\rm d}(t)]^2-\Gamma^2}(1+\eta(t)) \tag{46b}$$

with

$$\eta(t) \equiv \begin{cases} -\dfrac{\Gamma}{\sqrt{[2\omega_{\rm d}(t)]^2-\Gamma^2}}\tan^{-1}\dfrac{\sqrt{[2\omega_{\rm d}(t)]^2-\Gamma^2}}{\Gamma}, & |2\omega_{\rm d}(t)| > \Gamma \\ \dfrac{\Gamma}{2\sqrt{\Gamma^2-[2\omega_{\rm d}(t)]^2}}\ln\dfrac{\Gamma-\sqrt{\Gamma^2-[2\omega_{\rm d}(t)]^2}}{\Gamma+\sqrt{\Gamma^2-[2\omega_{\rm d}(t)]^2}}, & |2\omega_{\rm d}(t)| < \Gamma. \end{cases} \tag{47}$$

The vanishing of $n_{\rm d}^{(1)}(t)$ is due to the fact that $[\rho_{\rm d}^{\rm f}(t,\omega=0)]_{11} = [\rho_{\rm d}^{\rm f}(t,\omega=0)]_{12}$ [see equation (45)], implying that the normal and anomalous contributions (at the Fermi level) to the occupation cancel each other exactly. This cancellation results in the vanishing dissipation up to the order of Ω^2

$$P_{\rm dis}(t) = en_{\rm d}^{(1)}(t)\dot{V}(t) = 0 = R_{\rm q}[I^{(1)}(t)]^2 \tag{48}$$

or the zero relaxation resistance, $R_{\rm q} = 0$. It should be noted that this result coincides with that of the linear-response study [35]. In the linear-response analysis, the vanishing dissipation is attributed to the canceling in the particle–hole pair generation in the reservoir between the charge-conserving and pairing processes: the particle–hole pair amplitude of the two processes are same in magnitude but opposite in sign due to the fermion ordering. Such canceling effect is well manifested in equation (28b) which shows that the first-order correction to the occupation is proportional to the difference between the normal and anomalous contributions to the density of states. Consequently, the instantaneous Joule law with $R_{\rm q} = 0$ still holds in the cTSC phase.

Contrast to the QAH case, however, the Joule law, equation (48) is not valid for arbitrary values of $\epsilon_{\rm d}(t)$. For example, the current $I^{(1)}(t)$ [see equation (46b)] diverges logarithmically at $\epsilon_{\rm d}(t) = 0$, making it undefined: $I^{(1)}(t) \propto \ln|2\omega_{\rm d}(t)|/\Gamma$ for $|2\omega_{\rm d}(t)| \ll \Gamma$. In fact, as will be shown in the following numerical analysis, $R_{\rm q}$ diverges as $\Omega \to 0$ in the case $0 \in \mathcal{I}$, that is, for the ac driving which can make the dot crosses the Fermi level ($\epsilon_{\rm d}(t) = 0$). It is quite in contrast to the vanishing dissipation, equation (48), which holds only for the case $0 \notin \mathcal{I}$. This kind of singular behavior at resonance can be understood by considering the $\epsilon_{\rm d}(t) \to 0$ limit of the dot density of states:

$$[\rho_{\rm d}^{\rm f}(t,\omega)]_{11/12} \to \frac{1}{2}\delta(\hbar\omega) \pm \frac{1}{2\pi\hbar}\frac{\Gamma}{\omega^2+\Gamma^2}. \tag{49}$$

In order to explain the appearance of the half δ-peak, one needs to introduce the dot Majorana fermion operators: $\gamma_{d,1} = (d-d^\dagger)/\sqrt{2}i$ and $\gamma_{d,2} = (d+d^\dagger)/\sqrt{2}$. The dot and tunneling Hamiltonians then read

$$H_{\rm dot} = i\epsilon_{\rm d}(t)\gamma_{\rm d,2}\gamma_{\rm d,1} \tag{50a}$$

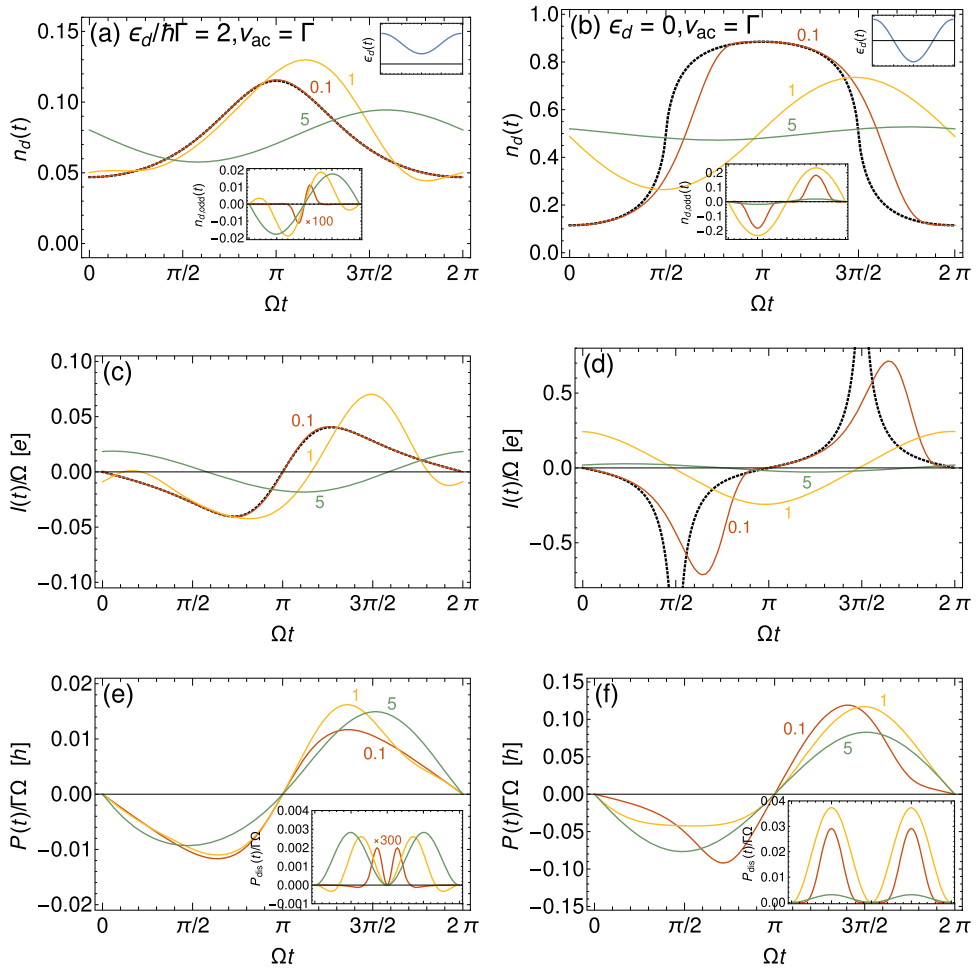

Figure 4. Time dependence of (a) and (b) the dot occupation $n_{\rm d}(t)$, (c) and (d) current $I(t)/\Omega$, and (e) and (f) the ac power $P(t)/\Gamma\Omega$ for (a), (c) and (e) $\epsilon_{\rm d} = 2\hbar\Gamma$ and $v_{\rm ac} = \Gamma$ and (b), (d) and (f) $\epsilon_{\rm d} = 0$ and $v_{\rm ac} = \Gamma$ with respect to the cTSC reservoir. The value of the ac frequency Ω/Γ for each curve is as annotated. The dotted lines correspond to those calculated by the adiabatic approximation. The insets in the upper-right corner of (a) and (b) displays the time variation of $\epsilon_{\rm d}(t)$ (here the horizontal line is the Fermi level) and those at bottom are the odd parts of the dot occupation. The insets in (e) and (f) are the even part of the ac power, responsible for the dissipation. $n_{\rm d,odd}(t)$ and $P_{\rm dis}(t)/\Gamma\Omega$ for $\Omega/\Gamma = 0.1$ in the insets are amplified for better presentation.

$$H_{\rm tun} = \sum_k \sqrt{2} i (t_2 \gamma_{{\rm d},2} \gamma_{k,2} - t_1 \gamma_{{\rm d},1} \gamma_{k,1}). \tag{50b}$$

It should be noted that the tunneling Hamiltonian, equation (50b) remains in the same form even if the tunneling amplitudes have the momentum dependence, $t_{1/2} \to t_{1/2,k}$ as long as they are real and symmetric, $t_{1/2,k} = t_{1/2,-k}$. Since $t_2 = 0$ (or $t_{2,k} = 0$) in the cTSC phase, the dot Majorana operator $\gamma_{{\rm d},2}$ is completely decoupled from the system for $\epsilon_{\rm d}(t) = 0$, making the half δ-peak contribution to the dot density of states. Whenever $\epsilon_{\rm d}(t)$ crosses the Fermi level, this singularity in the dot density of states affects the system critically, no matter how slow the ac driving is, and accordingly the adiabatic approximation fails. Therefore, even the adiabatic-limit study in the cTSC case requires the exact solving of equations (19) and (21), which is to be done in the next section.

4.2. Numerical calculation

Figure 4 displays the typical time dependence of the dot occupation, the current, and the ac power for the two cases, $0 \notin \mathcal{I}$ and $0 \in \mathcal{I}$, obtained by the exact numerical calculation. First, we check the validity of the adiabatic approximation obtained in the previous section. For the case $0 \notin \mathcal{I}$ [see figures 4(a) and (c)], for sufficiently small frequencies (say $\Omega/\Gamma = 0.1$), the adiabatic approximation is in good agreement with the exact results, while the discrepancy between two grows with increasing the ac frequency. In contrast, for the case $0 \in \mathcal{I}$, there is huge discrepancy between the results by the adiabatic approximation and the exact calculation even for the very small frequencies [see figures 4(b) and (d)]. The discrepancy increases as the dot level approaches the Fermi level, becoming maximal when $\epsilon_{\rm d}(t) = 0$: moreover, at $\epsilon_{\rm d}(t) = 0$, $I(t)$ from

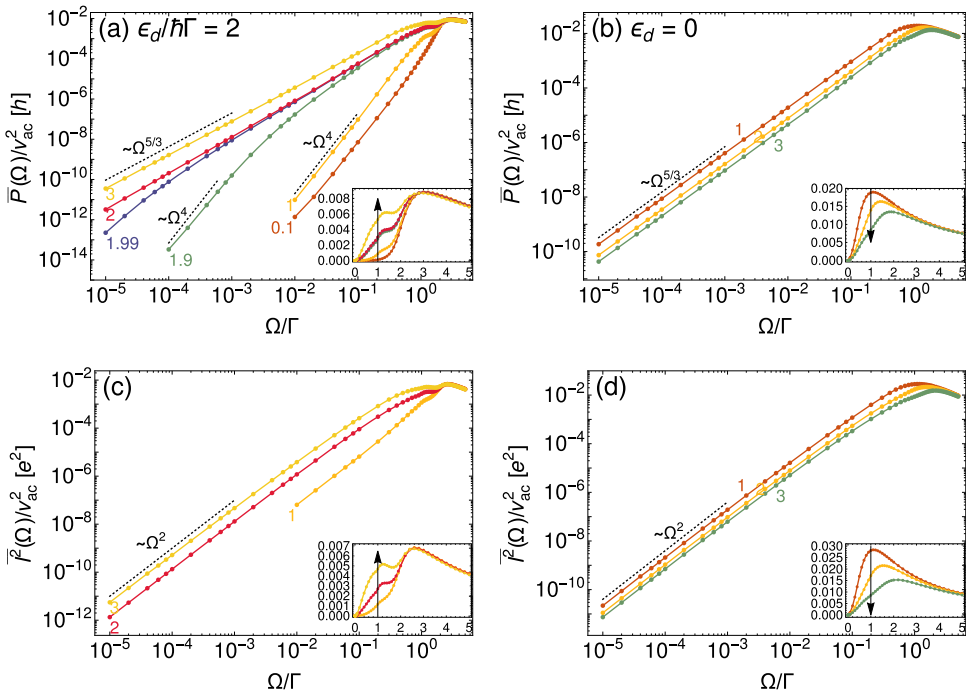

Figure 5. Logarithmic plots of (a) and (b) time-averaged ac power $\overline{P}/v_{ac}^2$ and (c) and (d) time-averaged squared current $\overline{I^2}/v_{ac}^2$ as functions of Ω for several values of v_{ac}/Γ (as annotated) for (a) and (c) $\epsilon_d = 2\hbar\Gamma$ and (b) and (d) $\epsilon_d = 0$ with respect to the cTSC reservoir. The insets show the corresponding linear-scale plots. The arrows indicate the direction along which the chosen values of v_{ac}/Γ increases.

the adiabatic approximation diverges. Therefore, as commented before, for the case $0 \in \mathcal{I}$, the adiabatic approximation is not valid.

On the other hand, interestingly, in the opposite limit, that is, for very large frequencies (say $\Omega/\Gamma = 5$) the response of the dot occupation and the current is quite sinusoidal with respect to the time t. It is similar to that of the linear-response theory. In general non-equilibrium situation, the ac response is non-sinusoidal because of the delayed response and the interplay between different energy scales. This sinusoidal behavior, therefore, is the another evidence supporting the argument in section 2.4 that at high frequencies the system reacts linearly.

Since the odd part of the ac power is time-averaged out, only its even part explains the dissipation [see the insets in figures 4(e) and (f)]. From the definition of the ac power, equation (7), and the odd nature of $\dot{V} \propto \sin \Omega t$, one can find that the odd part of the dot occupation, $n_{d,odd}(t)$ is responsible for the dissipation, which is displayed in the insets of figures 4(a) and (b). The results show us the time when the system is most dissipative. At low frequencies [see the case of $\Omega/\Gamma = 0.1$], most of the dissipation occurs when the system is closest to the resonance: for the case $0 \notin \mathcal{I}$, it happens at $\Omega t \approx \pi$ [see figure 4(e)] and for the case $0 \in \mathcal{I}$, at $t \approx t_R$ where $\epsilon_d(t = \pm t_R) = 0$ or $\Omega t_R = \cos^{-1}(-\epsilon_d/eV_{ac})$ [see figure 4(f) and in this case with $\Omega t_R = \pi/2$]. On the other hand, at high frequencies [see $\Omega/\Gamma = 5$ case], the maximal dissipation happens when $\dot{\epsilon}_d(t)$ (or $n_{d,odd}(t)$) is the largest in magnitude, that is, at $\Omega t \approx \pi/2, 3\pi/2$ for both $0 \notin \mathcal{I}$ and $0 \in \mathcal{I}$ cases.

Now we investigate the time-averaged values of $\overline{I^2}$ and $\overline{P}$ as functions of Ω and v_{ac}, which are shown in figure 5. The frequency dependence of $\overline{I^2}$ is quite similar to that in the QAH case [see figures 2(c) and (d)]: (1) at sufficiently low frequencies, $\overline{I^2} \propto \Omega^2$ and (2) in the intermediate range of frequencies, $\overline{I^2}$ is maximized around a frequency comparable to Γ. While the amplitude-normalized $\overline{I^2}/v_{ac}^2$ decreases with increasing v_{ac}, its raw value increases with increasing v_{ac} in both $0 \notin \mathcal{I}$ and $0 \in \mathcal{I}$ cases. This qualitative similarity in the current response of the QAH and cTSC reservoirs can be attributed to the fact that the current between the dot and the reservoir is driven directly by the gate voltage on the dot, making it less affected by the physical properties of the reservoir.

However, the dissipation in the cTSC reservoir is clearly different from that in the QAH reservoir, especially at low frequencies. In the case $0 \notin \mathcal{I}$ [see the cases of $v_{ac} < \epsilon_d/\hbar = 2\Gamma$ in figure 5(a)], $\overline{P}$ follows a power law, $\overline{P} \propto \Omega^4$ for small frequencies. The appearance of finite Ω^4 term is expected from the adiabatic approximation which predicted that $P_{dis}(t) = 0$ up to the second order of Ω, together with the fact that the odd powers of Ω of $P(t)$ belong to the conservative power and are time-averaged to zero.

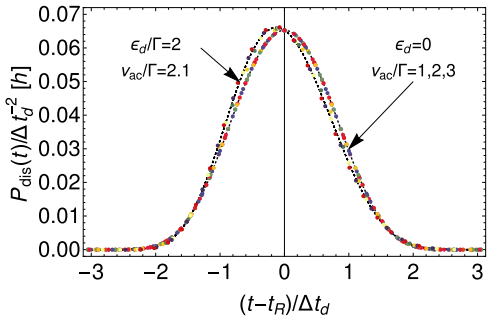

Figure 6. Scaled plot of $P_{\rm dis}(t)$ around $t = t_{\rm R}$ with respect to the cTSC reservoir [see the inset in figure 4(f)]. The points with different colors correspond to the results obtained from different values of $v_{\rm ac}$ and (sufficiently small) Ω. All the data, properly scaled, collapse into the corresponding single curves (depending on the value of $\tilde{b}$) which are fitted into Gaussian-like ones (black dotted lines) [see the text for detailed form of the fitted curves].

On the other hand, in the case $0 \in \mathcal{I}$ [see figure 5(b) and the cases of $v_{\rm ac} \geqslant \epsilon_{\rm d}/\hbar$ in figure 5(a)], the numerical calculation finds out that another power law is operative: $\overline{P} \propto \Omega^{\frac{5}{3}}$. In order to find out the origin of this interesting power law, we examine more carefully the time dependence of $P_{\rm dis}(t)$ at low frequencies. As seen in the inset of figures 4(e) and (f), $P_{\rm dis}(t)$ exhibits two peaks centered at $t = \pm t_{\rm R}$, implying that the dissipation is maximized at resonance. Interestingly, the numerical data shows that $P_{\rm dis}(t)$ around the peaks ($t = \pm t_{\rm R}$) follows a *universal scaling law* at sufficiently low frequencies, as can be seen in figure 6:

$$P_{\rm dis}(t) = \frac{h}{\Delta t_{\rm d}^2}\widetilde{P}\left(\frac{t \pm t_{\rm R}}{\Delta t_{\rm d}}, \frac{\epsilon_{\rm d}}{\hbar\Gamma}(\Delta t_{\rm d}^3\Gamma\Omega^2)^{\frac{5}{6}}\right), \tag{51}$$

where $\widetilde{P}(\tilde{t}, \tilde{b})$ is a dimensionless function, which is well fitted into a Gaussian-like form, $\widetilde{P}(\tilde{t}, \tilde{b}) = a_0 \exp\left[-a_2\tilde{t}^2 - a_4\tilde{t}^4 - \tilde{b}(a_1\tilde{t} - a_3\tilde{t}^3)\right]$ with $a_0 \approx 0.065$, $a_1 \approx 0.046$, $a_2 \approx 0.73$, $a_3 \approx 0.018$, and $a_4 \approx 0.071$. The parameters $\Delta t_d = |\dot{\epsilon}_d(t_R)/\hbar\Gamma^{\frac{1}{2}}|^{-\frac{2}{3}} = |\Omega v_{\rm ac}\ \sin\ \Omega t_R/\Gamma^{\frac{1}{2}}|^{-\frac{2}{3}} = |\Omega\sqrt{v_{\rm ac}^2 - (\epsilon_d/\hbar)^2}/\Gamma^{\frac{1}{2}}|^{-\frac{2}{3}}$ and $\tilde{b} = (\epsilon_d/\hbar\Gamma)(\Delta t_d^3\Gamma\Omega^2)^{\frac{5}{6}} = (\epsilon_d/\hbar\Gamma)(\sqrt{v_{\rm ac}^2 - (\epsilon_d/\hbar)^2}/\Gamma)^{-\frac{5}{3}}$ define the time interval during which most of the dissipation occurs and the measure of the asymmetry of the time distribution of the dissipation with respect to the peak, respectively. Note that $\tilde{b}$ is Ω-independent. For $\epsilon_{\rm d} = 0$, $\overline{P}$ becomes symmetric with $\tilde{b} = 0$, and the time-averaged ac power is calculated into

$$\overline{P} = \frac{2}{\tau}\int_{-\infty}^{\infty} {\rm d}t P_{\rm dis}(t) = 2h\frac{\Omega}{2\pi}\frac{\Delta t_{\rm d}}{\Delta t_{\rm d}^2}\int_{-\infty}^{\infty} {\rm d}\tilde{t}\,\widetilde{P}(\tilde{t}, \tilde{b} = 0) \propto \frac{v_{\rm ac}^{\frac{2}{3}}\Omega^{\frac{5}{3}}}{\Gamma^{\frac{1}{3}}} \tag{52}$$

which explains Ω and $v_{\rm ac}$ dependence of $\overline{P}$ at low frequencies: $\overline{P}/v_{\rm ac}^2 \propto v_{\rm ac}^{-\frac{4}{3}}\Omega^{\frac{5}{3}}$ so the normalized dissipation decreases with increasing $v_{\rm ac}$. For $\epsilon_{\rm d} \neq 0$ or $\tilde{b} \neq 0$, $\overline{P}$ acquires non-trivial dependence on $v_{\rm ac}$, but still one can find that $\overline{P} \propto \Omega^{\frac{5}{3}}$.

The scaling law for the case $0 \in \mathcal{I}$ tells us that the dissipation occurs during a very small fraction of the period around the resonance: $\Delta t_{\rm d}/\tau \propto \Omega^{\frac{1}{3}}$, which becomes the smaller for the smaller frequencies. In addition, the fact that the time $\Delta t_{\rm d}$ depends only on the value of $\dot{\epsilon}_{\rm d}(t)$ at $t = t_{\rm R}$ suggests that this universal scaling is attributed to the resonance, that is, the scale-less δ-peak in the density of states [see equation (49)]. The infinitely enhanced density of states only near resonance greatly boosts the generation of the particle–hole pair into the reservoir and increases the dissipation even when the ac bias is very slowly varying with time: note that $\Omega^{\frac{5}{3}} \gg \Omega^4$ for small frequencies. While the singularity of the density of states at resonance explains the observed peculiar scaling behavior, it also, unfortunately, defies any analytical explanation for the fractional exponent 5/3 because any expansion technique does not work at resonance.

For the last comment on $\overline{P}$, we go back to the case $0 \notin \mathcal{I}$ but when the resonance is very close to one of the boundaries of $\mathcal{I}$: for example, see the cases of $v_{\rm ac}/\Gamma = 1.9$ and 1.99 in figure 5(a). As discussed before, $\overline{P} \propto \Omega^4$ for sufficiently low frequencies. However, as $|\epsilon_{\rm d}/\hbar \pm v_{\rm ac}| \to 0$, the Ω^4-region appears for the much smaller frequencies, and instead, in the intermediate frequencies, $\overline{P}$ behaves as in the $0 \in \mathcal{I}$ case: $\overline{P}$ exhibits the Ω-dependency close to $\Omega^{\frac{5}{3}}$, which is more clearly seen as $v_{\rm ac}$ approaches $\epsilon_{\rm d}/\hbar$ [see the case of $v_{\rm ac}/\Gamma = 1.99$ in figure 5(a)]. This behavior which happens when the ac driving is relatively fast may be attributed to the boosted Landau–Zener transition: the probability of the transition to the states close to resonance is enhanced so that the enhanced density of states near resonance becomes effective in the transport and the dissipation. Numerical calculations find that this intermediate frequency region featuring

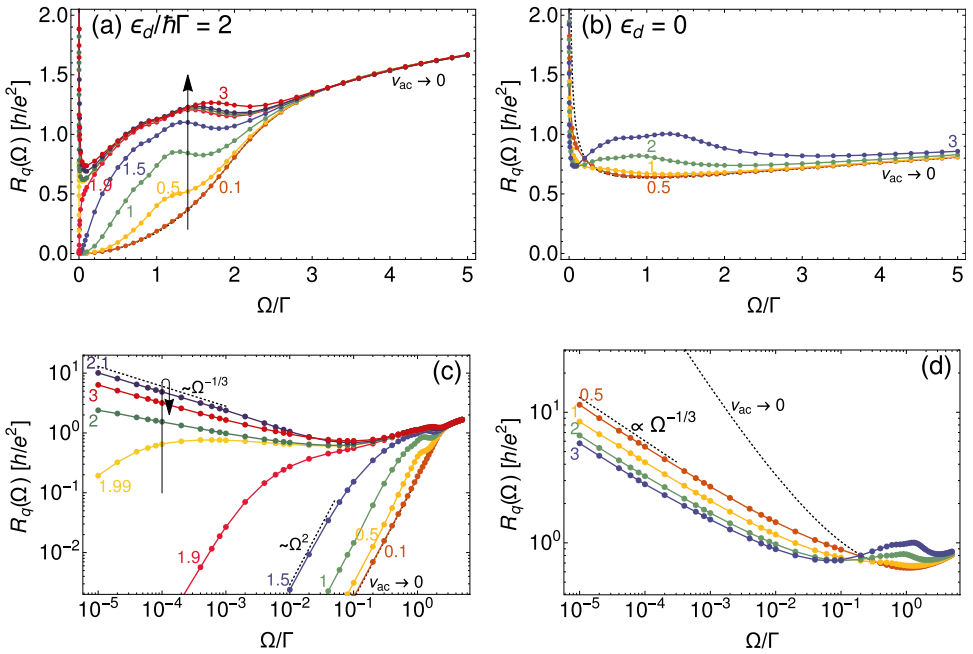

Figure 7. (a) and (b) Linear-scale and (c) and (d) logarithmic-scale plots of relaxation resistance R_q as a function of Ω for several values of v_{ac}/Γ as annotated for (a) and (c) $\epsilon_d = 2\hbar\Gamma$ and (b) and (d) $\epsilon_d = 0$, obtained by using the data in figure 5. The black dotted line represents the linear-response result ($v_{ac} \to 0$).

the $\Omega^{\frac{5}{3}}$ dependency expands into the lower frequency exponentially with respect to $|\epsilon_d/\hbar \pm v_{ac}|$, reaching up to the zero frequency when $\epsilon_d/\hbar \pm v_{ac} = 0$.

Finally, we examine the relaxation resistance R_q as the measure of the dissipation, which is displayed in figure 7. For not small frequencies ($\Omega/\Gamma \gtrsim 1$), a few general statement about R_q can be made whether $0 \notin \mathcal{I}$ or $0 \in \mathcal{I}$: (1) numerical calculation is in good agreement with the linear-response predication [35] in the $V_{ac} \to 0$ limit, (2) R_q increases with increasing v_{ac}, and (3) for sufficiently large frequencies, R_q follows the linear-response behavior for all values of the amplitude V_{ac}. These properties are quite similar to those for the QAH reservoir, implying that the dissipation for relatively large frequencies ($\Omega/\Gamma \gtrsim 1$) cannot distinguish between the QAH and cTSC reservoirs.

For small frequencies, however, R_q features the frequency dependence clearly different from the QAH case. First, for $0 \notin \mathcal{I}$, since $\overline{P} \propto \Omega^4$ and $\overline{I} \propto \Omega^2$, $R_q = \overline{P}/\overline{I^2} \propto \Omega^2$ and decreases to zero in the $\Omega \to 0$ limit. The vanishing of $R_q(\Omega = 0)$ matches well with that predicted by the adiabatic approximation and is valid regardless of the values of ϵ_d and v_{ac}, as long as $0 \notin \mathcal{I}$. It is also observed that the magnitude of R_q increases with increasing the ac amplitude v_{ac}, exhibiting a quite non-linear dependence on v_{ac}. For $0 \in \mathcal{I}$, on the other hand, since $\overline{P} \propto \Omega^{\frac{5}{3}}$ and $\overline{I} \propto \Omega^2$, $R_q \propto \Omega^{-\frac{1}{3}}$, indicating that $R_q \to \infty$ as $\Omega \to 0$. This divergence was also predicted in the linear-response study [35] [see the dotted line in figure 7(d)]. This diverging resistance at low frequencies is definitely attributed to a decoupled dot Majorana mode ($\gamma_{d,2}$) with the infinitely large density of states near zero energy and the elongated time for the dot to stay near resonance for slower ac oscillations. Note that the dot electron is coupled equally to the particle and hole components of the single Majorana edge mode so that the Majorana nature, leading to the proliferation of the particle–hole pairs, is highly enhanced at the resonant condition. Interestingly, for $0 \in \mathcal{I}$, R_q decreases with increasing v_{ac} [see the arrow in figure 7(c)]. It may be attributed to the decrease in the time for the dot to remain near the resonance with increasing v_{ac} at given Ω: note that $\Delta t_d \propto (v_{ac}^2 - (\epsilon_d/\hbar)^2)^{-\frac{1}{3}}$. Since most of the dissipation happens only near the resonance, the decreased Δt_d surely decreases R_q.

Our non-equilibrium study predicts that the diverging R_q obeys a scale-free power law $\propto \Omega^{-\frac{1}{3}}$, for all values of v_{ac} as long as $0 \in \mathcal{I}$ [see figures 7(c) and (d)]. The linear-response study at $\epsilon_d = 0$, however, predicted more complex frequency dependence: $R_q \propto 1/\Omega(\ln \Omega)^2$ at $\epsilon_d = 0$ [35] [see the dotted line in figure 7(d)]. Now we know that this logarithmic dependence is an artifact of the linear-response study: The linear-response approach assumes the equilibrium effectively so at $\epsilon_d = 0$ the dot remains on resonance at all time and the δ-peak dot density of states, equation (49), is used to calculate the relaxation resistance. However, it is not true in true non-equilibrium condition. Even for very small ac amplitude, $\epsilon_d(t) = \epsilon_d + eV(t)$ is finite at most of the time. Accordingly, the dot density of states, equation (45), varies with time. Especially, its value at $\omega = 0$ varies greatly even for small change in $\epsilon_d(t)$: the shape of the density

of states alters between the δ-peak ($\epsilon_{\rm d}(t) = 0$) and the sharp but finite peak ($\epsilon_{\rm d}(t) \neq 0$). It should be noted that this kind of artifact does not take place in the QAH reservoir because the dot density of state has no singular feature even at resonance.

5. Conclusion

In closing we have analyzed a topological RC circuit, a device manufactured by a quantum dot tunnel-coupled to a Majorana edge mode that is generated around a chiral topological superconductor. We have considered the scenario in which the dot is driven by a time-dependent dot gate potential and investigated the charge current and the associated dissipation that is represented by the ac power and the charge relaxation resistance. The exact non-equilibrium transport properties have been thoroughly examined within the nonequilibrium Keldysh Green function formalism and by using exact numerical integration. In the adiabatic regime the analytical forms of the physical quantities are available, helping clarifying the effect genuine to Majorana physics.

In contrast to the QAH reservoir for which the low-frequency relaxation resistance remains fixed at the universal value $R_{\rm q} = R_{\rm Q}/2$ for arbitrary values of the ac driving $V_{\rm ac}$ and the dot level $\epsilon_{\rm d}$, the dissipation through the Majorana edge mode is found to be dramatically sensitive to their values. Specifically, it changes abruptly depending whether the time-dependent dot level $\epsilon_{\rm d}(t) = \epsilon_{\rm d} + eV(t)$ crosses the Fermi level during the ac cycle or not. If the dot is kept away from the resonance for a whole ac cycle, the low-frequency resistance vanishes with decreasing the ac frequency Ω as $R_{\rm q} \propto \Omega^2$, which is attributed to the canceling effect of particle–hole pairs from two different processes. On the other hand, when the dot can be on resonance even temporally, the relaxation resistance features a singular behavior with the scaling law $R_{\rm q} \propto \Omega^{-1/3}$ with the exotic exponent. The reason for such singular behavior, not captured by the adiabatic approximation, is found in the existence of a δ-peak dot density of states due to the decoupling of a dot Majorana fermion from the reservoir on resonance. We found that this decoupling originates from the Majorana nature of the edge mode, being immune to non-essential complexities such as the momentum-dependent dot-reservoir tunneling amplitudes and the detailed form of the energy dispersion relation of the edge mode. Unfortunately, the physical explanation of the interesting power-law exponent $-\frac{1}{3}$ is currently not available and to be studied in the future.

We therefore propose the topological RC circuit as a probe of chiral Majorana edge modes. Its singular behavior with the exotic power-law exponent can unambiguously detect the existence of the Majorana modes. In experimental point of view, the measurement of the relaxation resistance in the RC circuit may be challenging [43], but our setup is non-invasive to the Majorana modes in that it requires only the tunneling junction to a quantum dot and no direct contact to other metallic probes which can degrade the formation of Majorana modes.

Data availability statement

All data that support the findings of this study are included within the article (and any supplementary files).

Acknowledgments

RL was supported by the MICINN/FEDER/MCIU/AEI Grant No. MAT2017-82639 and the Mara de Maeztu Program for Units of Excellence in RD (MDM-2014-0377 and MDM-2017-0711). ML was supported by the National Research Foundation of Korea (NRF) Grant funded by the Korea government (MSIT) (No 2018R1A5A6075964).

References

[1] Hasan M Z and Kane C L 2010 *Rev. Mod. Phys.* **82** 3045
[2] Qi X-L and Zhang S-C 2011 *Rev. Mod. Phys.* **83** 1057–110
[3] Kitaev A Y 2001 *Phys.-Usp.* **44** 131–6
[4] Alicea J 2012 *Rep. Prog. Phys.* **75** 076501
[5] Leijnse M and Flensberg K 2012 *Semicond. Sci. Technol.* **27** 124003
[6] Beenakker C W J 2013 *Annu. Rev. Condens. Matter Phys.* **4** 113–36
[7] Elliott S R and Franz M 2015 *Rev. Mod. Phys.* **87** 137–63
[8] Stanescu T, Lutchyn R and Das Sarma S 2011 *Phys. Rev.* B **84** 144522
[9] Nayak C, Simon S H, Stern A, Freedman M and Das Sarma S 2008 *Rev. Mod. Phys.* **80** 1083–159
[10] Aasen D *et al* 2016 *Phys. Rev.* X **6** 031016
[11] Mourik V, Zuo K, Frolov S M, Plissard S R, Bakkers E P A M and Kouwenhoven L P 2012 *Science* **336** 1003–7

[12] Das A, Ronen Y, Most Y, Oreg Y, Heiblum M and Shtrikman H 2012 *Nat. Phys.* **8** 887–95
[13] Deng M T, Yu C L, Huang G Y, Larsson M, Caroff P and Xu H Q 2012 *Nano Lett.* **12** 6414–9
[14] Churchill H O H, Fatemi V, Grove-Rasmussen K, Deng M T, Caroff P, Xu H Q and Marcus C M 2013 *Phys. Rev.* B **87** 241401
[15] Finck A D K, Van Harlingen D J, Mohseni P K, Jung K and Li X 2013 *Phys. Rev. Lett.* **110** 126406
[16] Nadj-Perge S, Drozdov I K, Li J, Chen H, Jeon S, Seo J, MacDonald A H, Bernevig B A and Yazdani A 2014 *Science* **346** 602–7
[17] Feldman B E, Randeria M T, Li J, Jeon S, Xie Y, Wang Z, Drozdov I K, Andrei Bernevig B and Yazdani A 2017 *Nat. Phys.* **13** 286–91
[18] Chen J, Woods B D, Yu P, Hocevar M, Car D, Plissard S R, Bakkers E P A M, Stanescu T D and Frolov S M 2019 *Phys. Rev. Lett.* **123** 107703
[19] Jiang L, Pekker D, Alicea J, Refael G, Oreg Y and von Oppen F 2011 *Phys. Rev. Lett.* **107** 236401
[20] Rokhinson L P, Liu X and Furdyna J K 2012 *Nat. Phys.* **8** 795–9
[21] Qi X L, Hughes T L and Zhang S C 2010 *Phys. Rev.* B **82** 184516
[22] Žitko R 2011 *Phys. Rev.* B **83** 195137
[23] He Q L *et al* 2017 *Science* **357** 294–9
[24] Ji W and Wen X G 2018 *Phys. Rev. Lett.* **120** 107002
[25] Huang Y, Setiawan F and Sau J D 2018 *Phys. Rev.* B **97** 100501
[26] Yasuda K, Mogi M, Yoshimi R, Tsukazaki A, Takahashi K S, Kawasaki M, Kagawa F and Tokura Y 2017 *Science* **358** 1311–4
[27] Büttiker M, Thomas H and Prêtre A 1993 *Phys. Lett.* A **180** 364–9
[28] Büttiker M, Prêtre A and Thomas H 1993 *Phys. Rev. Lett.* **70** 4114–7
[29] Gabelli J, Fève G, Berroir J M, Plaçais B, Cavanna A, Etienne B, Jin Y and Glattli D C 2006 *Science* **313** 499–502
[30] Nigg S, López R and Büttiker M 2006 *Phys. Rev. Lett.* **97** 206804
[31] Lee M, López R, Choi M S, Jonckheere T and Martin T 2011 *Phys. Rev.* B **83** 201304
[32] Mora C and Le Hur K 2010 *Nat. Phys.* **6** 697–701
[33] Filippone M, Le Hur K and Mora C 2011 *Phys. Rev. Lett.* **107** 176601
[34] Khim H, Hwang S Y and Lee M 2013 *Phys. Rev.* B **87** 115312
[35] Lee M and Choi M S 2014 *Phys. Rev. Lett.* **113** 076801
[36] Golub A and Grosfeld E 2012 *Phys. Rev.* B **86** 241105
[37] Lee M 2019 *Curr. Appl. Phys.* **19** 246–50
[38] Liu C X, Qi X L, Dai X, Fang Z and Zhang S C 2008 *Phys. Rev. Lett.* **101** 146802
[39] Yu R, Zhang W, Zhang H-J, Zhang S-C, Dai X and Fang Z 2010 *Science* **329** 61–4
[40] Chang C-Z *et al* 2013 *Science* **340** 167–70
[41] Alomar M I, Lim J S and Sánchez D 2016 *Phys. Rev.* B **94** 165425
[42] Ludovico M F, Lim J S, Moskalets M, Arrachea L and Sánchez D 2014 *Phys. Rev.* B **89** 161306
[43] Fève G, Mahé A, Berroir J-M, Kontos T, Plaçais B, Glattli D C, Cavanna A, Etienne B and Jin Y 2007 *Science* **316** 1169–72